Bidirectional optical neuromodulation using capacitive charge-transfer

RUSTAMZHON MELIKOV, 1 D SHASHI BHUSHAN SRIVASTAVA, 1 ONURALP KARATUM, 1 D ITIR BAKIS DOGRU-YUKSEL, 2 D UGUR MERIC DIKBAS, BRAHIM HALIL KAVAKLI, 3,4 D AND SEDAT NIZAMOGLU^{1,2,*}

Abstract: Artificial control of neural activity allows for understanding complex neural networks and improving therapy of neurological disorders. Here, we demonstrate that utilization of photovoltaic biointerfaces combined with light waveform shaping can generate safe capacitive currents for bidirectional modulation of neurons. The differential photoresponse of the biointerface due to double layer capacitance facilitates the direction control of capacitive currents depending on the slope of light intensity. Moreover, the strength of capacitive currents is controlled by changing the rise and fall time slope of light intensity. This approach allows for high-level control of the hyperpolarization and depolarization of membrane potential at single-cell level. Our results pave the way toward advanced bioelectronic functionalities for wireless and safe control of neural activity.

© 2020 Optical Society of America under the terms of the OSA Open Access Publishing Agreement

1. Introduction

Bidirectional modulation of membrane potential can allow for initiation or stimulation of neural activity [1]. This control of membrane potential helps in switching on and off the neural networks to understand the brain activity or treat biological disfunctions [2–4]. Optogenetics, which combines genetics with optics, introduced a wide variety of transmembrane proteins that can stimulate or silence neural activity [5]. For example, channelrhodopsin, halorhodopsin, and archaerhodopsin are used for neural activation and archaerhodopsin-3, eNpHR, KR2 are used for suppression of neural activity [6,7]. However, since these ion channels or pumps are generally introduced via genetic modification by a viral vector delivery [1], such a structural variation is currently one of the main concerns for its clinical use.

Extracellular electrical stimulation of nerve cells is a non-genetic and clinically-approved method to control the neural activity [8]. To mitigate the toxicity from electrochemical reactions at metal-tissue interfaces, charge-balanced alternating current pulses (AC) were used for implantable neuroprostheses including cochlear implants, deep brain stimulators, spinal cord stimulators, and retinal implants [9–12]. Short-duration pulses are applied to neural tissue in a phase-locked fashion for stimulation [13]. To inhibit the target neurons, implants typically work indirectly by delivering excitation to populations of neurons by delivering high pulse rates that suffer from some undesirable side effects such as persistent refractory state [14].

Capacitive charge-transfer mechanism is a long-term applicable and safe method without any tissue or electrode damage for neural stimulation [8]. It is based on the perturbation of the ion concentration of the electrolyte via a time-varying electric field on the electrode surface [15]. These currents are based on the double layer capacitance. Light-activated capacitors

¹Department of Electrical and Electronics Engineering, Koc University, Istanbul 34450, Turkey

²Graduate School of Biomedical Sciences and Engineering, Koc University, Istanbul 34450, Turkey

³Molecular Biology and Genetics, College of Science, Koc University, Istanbul 34450, Turkey

⁴College of Engineering, Chemical and Biological Engineering, Koç University, Istanbul 34450, Turkey *snizamoglu@ku.edu.tr

(i.e., photocapacitors) using different material systems such as organic, inorganic, or hybrid semiconducting materials have been investigated and show promise for effective capacitive current generation [16–20]. The capacitive currents are used for photostimulation of a wide variety of neurons such as DRG neurons, oocytes and cancerous cell lines [16–21].

Pulse modulation is a widely used technique in bioelectronics for neuromodulation [22–24]. In general, electrical power gradients were utilized. Schoen et. al. demonstrated modulation of membrane potential under rising and falling voltage pulse modulations to excite neural cells attached to capacitive substrate [24]. In terms of optical modulation, square-waves have been generally applied for photostimulation [16–17,20,21]. However, the effect of variation of light power gradients on photocapacitive substrates were not investigated for photostimulation yet.

In this report, we demonstrate control of membrane depolarization and hyperpolarization by modulating the input signal (light pulse) waveforms, which allow for bidirectional modulation of the membrane potential via capacitive charge-transfer. For that we fabricated biointerfaces based on a biocompatible photoactive layer of P3HT:PCBM bulk heterojunction. In order to control the photoelectric response, we performed a systematic study of the negative and positive capacitive transient photocurrents by changing pulse waveforms from square to asymmetric trapezoidal shapes that enables high-level control of membrane depolarization and hyperpolarization on SH-SY5Y neuronal cells.

2. Methods

2.1. Materials

Poly(3-hexylthiophene-2,5-diyl) (P3HT) with regioregularity of 95.7% and a molecular weight of 57,467 g mol⁻¹, [6,6]-PPhenyl-C61-butyric acid methyl ester (PC61BM) with a molecular weight of 1,031 g mol⁻¹ were purchased from Ossila Ltd. And used as received. Other materials and processing chemicals such as Zinc acetate dihydrate $(Zn(CH_3CO_2)_2 \cdot 2H_2O)$ with molecular weight 183.48 g mol⁻¹, Ethanolamine (HOCH₂CH₂NH₂) with molecular weight 61.08 g mol⁻¹, 1,2 dichlorobenzene were purchased from Sigma Aldrich and used without any purification.

2.2. Photocapacitor preparation

Indium Tin Oxide (ITO) on glass substrates (side length, 20 mm; side length, 15 mm; thickness 1.1 mm; resistance, $14 - 16 \,\Omega.\text{cm}^{-2}$; Ossila) was cleaned with 10 wt% Sodium Hydroxide solution for 5 min, 2% by volume a specific tension-active agent in a water solution (HELLMANEX II, 3%) for 15 mins at 55 °C, DI water for 15 min, acetone for 15 mins and isopropyl alcohol for 15 mins using ultrasonic bath. The cleaned ITO on glass coated substrates were dried in oven at 50 °C and treated with UV-Ozone for 15 min. ZnO precursor sol-gel solution (0.45 M) was prepared by mixing 219.3 mg Zinc acetate dehydrate (Zn(CH₃CO₂)₂·2H₂O), 2 ml of 2-Methoxyethanol (C3H₅O₂) and 73 mg of Ethanolamine (HOCH₂CH₂NH₂) and ultrasonicating at 55 °C for 15 min [2]. 20 mg ml⁻¹ of the donor co-polymer P3HT and 10 mg ml⁻¹ of acceptor molecule PC61BM solution was prepared in o-dichlorobenzene and stirred overnight at 70 °C on a hot plate. Then, 20 mg ml⁻¹ P3HT and 10 mg ml⁻¹ PC61BM (1:0.5 wt. ratio) was mixed and stirred at 70 °C for 4 hours. The optimized photoelectrode was fabricated by spin coating ZnO precursor sol-gel solution at 2000 rpm for 60 s on a cleaned ITO coated on glass substrate and annealed on a hot plate at 290 °C for 15 min [3]. Further on ITO/ZnO substrate photoactive blend of P3HT:PC61BM (1:0.5 wt. ratio) solution in o-dichlorobenzene was spin coated at 1000 rpm for 90 s, then heated at 150 °C for 15 min.

2.3. Optical and surface characterization

UV-Vis Transmittance (Edinburg) was used to measure absorbance of the optimized photoelectrode. Scanning electron microscopy (SEM) (Zeiss) was used for imaging surface profile and the cross-sectional structure of the optimized photocapacitor.

2.4. Photocurrent measurements

The photocurrent measurements were performed on a set up including an Olympus T2 upright microscope. An extracellular patch clamp (EPC) 800 patch clamp amplifier (HEKA Elektronik) is used for measuring photocapacitive currents. The experiment was carried out at room temperature in an extracellular artificial cerebrospinal fluid (aCSF) aqueous medium as supporting electrolyte solution. Extracellular medium of aCSF was prepared by mixing 10 mM of 4-(2-hydroxyethyl)1-piperazineethanesulfonic acid (HEPES), 10 mM of glucose, 2 mM CaCl₂, 140 mM of NaCl, 1 mM of MgCl₂, 3 mM of KCl, into the distilled water and pH was calibrated to 7.4 using 1M NaOH. For the light stimulation, Thorlab's blue LED (M450LP1) with nominal wavelength of 445 nm was used at intensity level of 150 mW. cm⁻². LED were driven by DC2200 - High-Power 1-Channel LED Driver with Pulse Modulation (Thorlab's). A power meter (Newport 843-R) was used to measure the exact power of light reaching the surface of photocapacitor. The illumination was focused with water immersion objective. Illumination area was 1×1 cm². The photocapacitor corners were cleaned with toluene to stabilize the photocurrent measurements.

2.5. Electrophysiology

Electrophysiology measurements were performed with EPC 800 patch clamp amplifier (HEKA Elektronik). The photocapacitors were cleaned with 70% (by volume) ethanol solution and incubated for 2 day in water. The pulled patch pipettes of 8-12 MΩ were used to perform the whole-cell patch clamp experiment. Extracellular medium aCSF was prepared as previous mentioned. Internal cellular medium was prepared by mixing 140 mM KCl, 2 mM MgCl², 10 mM HEPE, 10 mM ethylene glycol-bis(β-aminoethyl ether)-N,N,N',N'-tetraacetic acid (EGTA), 2 mM Mg-ATP in water and its pH was calibrated to 7.2-7.3 using 1 M KOH, and patch pipettes were filled with intracellular solution. Digital camera integrated with Olympus T2 upright microscope was used to monitor the cells. For the cell growth on the biointerface we used the cell culture methodology as in Ref. [21]. SHSY-5Y neuroblastoma cell line was used for electrophysiology. Dulbecco's Modified Eagle's Medium (DMEM, Gibco 41966-029) with 10% heat-inactivated fetal bovine serum (FBS, Gibco 10500) and antibiotics (1% penicillin-streptomycin, Gibco 15240-062) was used as a growth medium. The cells were cultured at 85% humidified incubator at 37 0 C with 5% CO₂.

2.6. Optical safety considerations

According to ocular safety standards for ophthalmic applications, the maximum permissible radiant power (MPF) that could enter the pupil chronically or in a single short exposure is calculated. For single-pulse exposures (pulse width of 10ms) at 400 - 700 nm, the peak limit is governed by the equation MPF = 6.93 \times 10-4 C_TC_E t-0.25, where, t = 10 ms (pulse width), C_T = 1 in the range of 400–700 nm and C_E is a function of the visual angle α . For retinal spot sizes greater than 1.7 mm, α = α max = 100 mrad and C_E = 6.67 \times 10-3 α^2 = 66.7 W. For 10 ms pulse width MPF = 146.17 mW. For a pupil size with diameter 1.7 mm MPF per unit area is MPFper unit area = 6443 mW. cm $^{-2}$.

3. Results and discussion

3.1. Biointerface characterization

We fabricated a capacitive charge-injecting biointerface developed by Srivastava et. al. [21], which is comprised of ITO on top of glass substrate as the back electrode, ZnO as the electron transport layer, and P3HT:PC61BM blend thin film as the photoactive layer (Fig. 1(a)). The cross-sectional SEM image shows that the thickness of the photoactive layer is ~ 100 nm and the thickness of the ZnO layer is ~ 50 nm (Fig. 1(b)). The energy band alignment (Fig. 1(c)) reveals that the electron transport is favorable towards ZnO and hole transport towards P3HT. The absorption spectra of the photocapacitor (Fig. 1(d)) advantageously covers almost the whole visible range that originate by the collective absorption of the bulk heterojunction composites from violet to red spectral window and ZnO layer in the ultra-violet region.

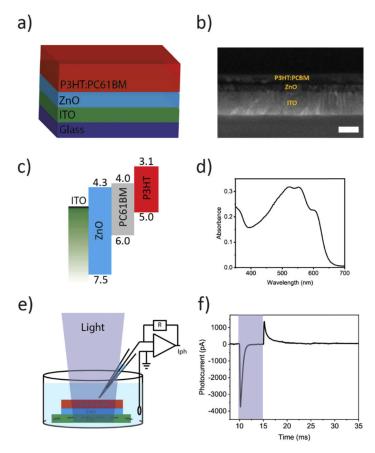


Fig. 1. (a) Schematic of device structure of the photocapacitor (ITO/ZnO/P3HT:PC61BM). (b) Cross-sectional SEM image of photocapacitor. (c) Energy band diagram of the photocapacitor. (d) Ultraviolet-to-visible (UV-Vis) absorbance spectrum of ZnO/P3HT:PC61BM thin film. (e) Schematic of the photocurrent measurement set-up. The patch pipette is kept close to the surface and the current is measured with a voltage-clamp mode under free-standing configuration. (f) Photocurrent under 5 ms pulsed illumination.

After the incoming light-radiation in the visible range is absorbed by the photoactive blend, the photogenerated charge carriers dissociate due to the band alignment. Electrons are drifted toward ITO and holes are localized in the P3HT to induce a displacement current. Here the integration of the intermediate layer of ZnO between ITO and the photoactive layer decreases the strength of

the Faradaic portion of the photocurrent [21]. Moreover, ZnO thin film acts as a hole blocking layer, which reduces electron-hole recombination and thereby, it enhances the output capacitive photocurrent. Since LUMO energy of P3HT is above water oxidation energy, Faradaic current due to hole transfer into the electrolyte is significantly suppressed. Hence, the hole accumulation in the biointerface close to the electrolyte can generate a capacitive photocurrent.

3.2. Biointerface photoresponse

The photocapacitor was probed for the photocurrent response inside the aCSF solution using patch-clamp system (HEKA, EPC800) in voltage-clamp mode with $\sim 6~M\Omega$ patch pipette tips in free-standing condition (Fig. 1(e)). We built an optomechanical setup that allowed light illumination from the top side on the biointerface surface impinging initially on the photoactive layer (Fig. 1(e)). First, we characterized the photocapacitor with 5-ms square-wave blue light illumination at the peak intensity level of 150 mW cm⁻² and found the capacitive photocurrent with asymmetric negative spike of 3.86 nA and positive spike of 1.35 nA, respectively (Fig. 1(f)). Since the holes mainly attract negative ions and repulse the positive ions, the light rise-time induces a negative capacitive transient current that corresponds to a direction from electrode to electrolyte. In contrast, while the light is turned off, since the hole accumulation and potential decreases due to recombination of photogenerated charge carriers, a positive current spike is observed. Rand et. al. [17] reported 17 mV transmembrane potential change by a photocapacitor consisting of sequentially deposited Cr/Au and H2Pc (p-type) and PTCDI (n-type). Abdullaeva et. al. [19]. reported photocurrent levels of 100 pA and transmembrane potential change up to 100 µV by using SQIB:PCBM photocapacitor. Hence, the photocurrents and transmembrane potential changes reported in this study are at comparable levels.

In order to study the controlling behavior of the shape of light pulse waveform on capacitive photocurrents, we varied input light waveforms from square to asymmetric trapezoidal shapes.

For that we changed the illumination rise time (t_2) in Fig. 2(a) from 250 µs to 20 ms while keeping t_1 ($t_1 = 5$ ms) fixed at the peak light intensity of 150 mW cm⁻². Under these conditions, the negative peak decreased from 1720 pA to 410 pA while the slope changed from 600 mW cm⁻² ms⁻¹ to 7.5 mW cm⁻² ms⁻¹, respectively (Fig. 2(c)). The photocurrent during the termination of light was relatively constant around 1.35 nA.

Similarly to analyze the effect of illumination fall time on the capacitive photocurrent, trapezoidal light pulse was used to illuminate the biointerface having 5-ms constant illumination of 150 mW cm⁻² ($t_1 = 5$ ms) while the fall time of t_2 was varied from 250 μ s to 20 ms in Fig. 2(b) that corresponds to the illumination slopes ranging from 600 mW cm⁻² ms⁻¹ to 7.5 mW cm⁻² ms⁻¹. The negative peak of the measured photocurrent remained relatively constant at the level of 3.86 nA, and the positive peak decreased from 572 pA to 244 pA for the slopes ranging from 600 mW cm⁻² ms⁻¹ to 7.5 mW cm⁻² ms⁻¹ fall time, respectively (Fig. 2(b), 2(d)).

To analyze the photocurrent trends, we mathematically fitted the negative and positive current peaks with R^2 =98.6% and 99.5%, respectively (Fig. 3(a) and 3(b)). Maximum negative and positive capacitive transient peaks are 3860 pA and 1350 pA that are generated by square response of LED driver (Fig. 1(f)). Here the slope of the square wave is limited by the illumination system. According to the fits of Eqs. (1) and 2, the maximum rise and fall time limited by the illumination system were calculated as 101.7 ns and 102.1 ns showing the square-wave response, which correspond to the slopes of 1430 W cm⁻² ms⁻¹ and 1437 W cm⁻² ms⁻¹. Moreover, using fitted Eqs. (1) and 2, we can also predict light intensity rate to obtain desired negative and positive capacitive transient peaks. For example, to obtain negative capacitive transient current peak of 38.6 pA (1% of the maximum negative capacitive transient current peak of the square-wave photoresponse) the light intensity rate should be 1.0 mW cm⁻² ms⁻¹, which corresponds to t_2 of 115.4 ms. Similarly, to obtain positive capacitive transient current peak of 13.5 pA (1% of the maximum positive capacitive transient current peak of the square-wave photoresponse) the

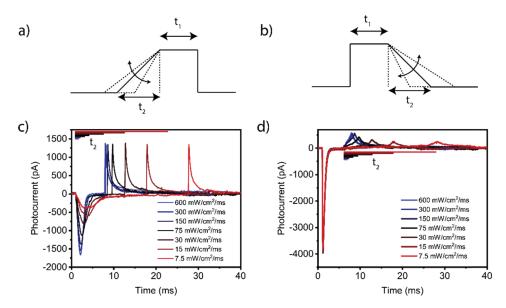


Fig. 2. Photocurrents generated by the photocapacitors under free-standing mode. (a) Pulse waveforms modulating the negative capacitive transient part of the photocurrent. (b) Pulse waveform modulating the positive capacitive transient part of the photocurrent. (c) Modulation of negative capacitive transients under different intensity slopes. (d) Modulation of positive capacitive transients under different intensity slopes.

light intensity rate should be 1.3 mW cm⁻² ms⁻¹, which corresponds to t_2 of 144.2 ms. While the negative and positive peaks were varied, the amount of charge was constant around 1.2 pC (Fig. 3(c) and 3(d)).

$$y(pA) = -47.13 + 618.49 \ln\left(x\left(\frac{mW}{cm^2ms}\right)\right)$$
 (1)

$$y(pA) = -1.00 + 218.57 \ln \left(x \left(\frac{mW}{cm^2 ms} \right) \right)$$
 (2)

While linear rising or falling voltage ramps generate constant capacitive currents in electrical stimulation, the case for light-evoked optoelectronic biointerfaces is different. When the photoelectrode is interfaced with the electrophysiological media in the wireless mode, it operates more closely under the open-circuit condition like a solar cell. Hence, we can consider that the conduction current is approximately zero and $V \approx V_{oc}$. Since this case analogically corresponds to the shunt resistance much larger than the series resistance in wired photovoltaic devices, Open circuit voltage (V_{oc}) can be approximated as in Eq. (3), which shows a logarithmic relation with the light intensity (P_{opt}) [25]. Since the capacitive current is proportional with the derivative of the voltage (i.e., photovoltage or open-circuit voltage) (Eq. (4)–(5)), the capacitive current is proportional with the first derivative of logarithm of applied light intensity.

$$V_{oc} \propto \frac{nk_BT}{q}ln(P_{opt}) \tag{3}$$

$$I_{cap} \propto C \frac{d}{dt}(V)$$
 (4)

$$I_{cap} \propto \frac{d}{dt}(V_{ph}) \propto \frac{d}{dt}(V_{oc}) \propto \frac{d}{dt}(\ln(P_{opt}))$$
 (5)

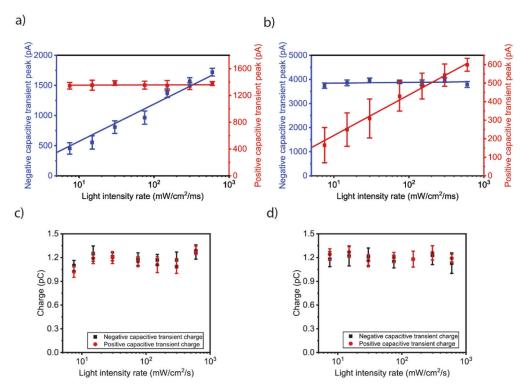


Fig. 3. (a) Negative capacitive transient peaks (blue squares) under different light intensity slopes. Since the illumination fall time are kept constant, the positive capacitive peaks (red squares) remained at similar level. Blue and red line is the fit with R^2 as 99.4% and 99.5%, respectively. (b) Positive capacitive transient peaks (blue squares) under different light intensity slopes. Since the illumination fall time are kept constant, the negative capacitive peaks (red squares) remained at similar level. Blue and red line is the fit with R^2 as 99.8% and 98.6%, respectively. (c)-(d) Negative and positive transient charges under different light intensity slopes. (N = 3 and error bars show the relative standard deviation.)

3.3. Photostimulation of neurons

To investigate the electrophysiological cellular photoresponse, we performed the patch clamping of SHSY-5Y cells seeded on the biointerface in whole-cell configuration (Fig. 4(a)). The I-V characteristics of SHSY-5Y cells grown on photocapacitor under dark condition was performed in voltage clamp mode, which shows that the SHSY-5Y cells exhibit typical resting membrane potential in the range of -20 to -50 mV (Fig. 4(b)). The SHSY-5Y cells exhibits quasi-linear response around the resting membrane potential. Under pulsed illumination we see depolarization followed by hyperpolarization of the membrane potential with photocapacitor having first negative transient current peak followed by positive transient current peak. Fromherz and co-workers demonstrated in their analysis that depolarization occurring at junction membrane results hyperpolarization at free membrane (or vice versa) [24]. Since the junction membrane is attached to photoelectrode, we observe first depolarization then hyperpolarization at the free-membrane. Moreover, the biointerface does not induce any toxicity on cells in-vitro [21].

The change in membrane potentials under light modulation is shown in Fig. 4(c) and 4(d). When the biointerface was illuminated by a trapezoidal pulse that has a rise time (t_2) ranging from 250 μ s to 20 ms corresponding to the rising slope from 600 mW cm⁻² ms⁻¹ to 7.5 mW cm⁻²ms⁻¹, the depolarization of the membrane potential peak decreased from 11.9 mV to 3.1 mV

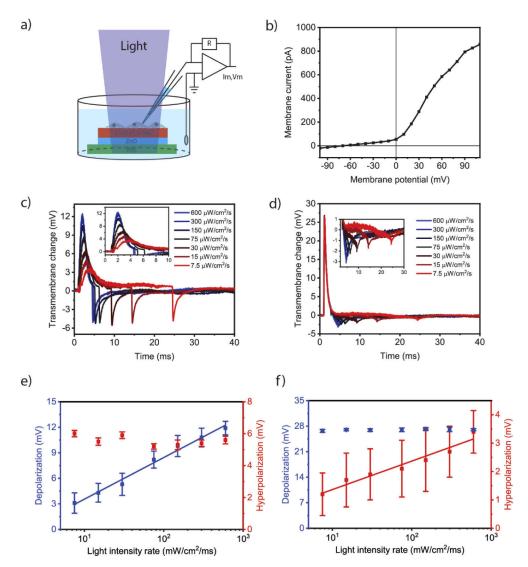


Fig. 4. (a) Schematic of the whole-cell patch clamp recording configuration. The cells are grown on the photocapacitor and adhere on the surface. Collimated LED is used to illuminate and activate the photocapacitor. (b) Current-voltage characteristics of a typical SHSY-5Y cell on the photocapacitor. (c) Transmembrane potential change vs time of the SHSY-5Y cells on the photocapacitor with different levels of negative capacitive transient modulation. (d) Transmembrane potential change vs time of the SHSY-5Y cells on the photocapacitor with different levels of positive capacitive transient modulation. (e) Depolarization and hyperpolarization peak under different levels of negative capacitive transient modulation. Blue line is the fit with an R^2 of 99.4%. (f) Depolarization and hyperpolarization peak under different levels of positive capacitive transient modulation. Blue line is the fit with an R^2 of 97.4. (N = 3 and error bars show the relative standard deviation.)

under, respectively (Fig. 4(e)). The depolarization peak of the membrane varied logarithmically under variation of the rise time slope with $R^2 = 98.6\%$ fit (see Fig. 4(e)) (see Eq. (6)). At the same time, hyperpolarization membrane potential remained constant as 5.6 mV due to the keeping the fall time fixed. Furthermore, for the trapezoidal pulse that has variation in fall time from 600 mW cm⁻² ms⁻¹ to 7.5 mW cm⁻² ms⁻¹ and constant rise time, the depolarization of membrane potential remained relatively constant as 27 mV and hyperpolarization of membrane potential decreased from 3.4 mV to 1.2 mV, respectively (Fig. 4(f)). The hyperpolarization peak of the membrane potential varied logarithmically under variation of the fall time slope with R^2 of 99.5% fit (see Fig. 4(f)) (see Eq. (7)). Under variation of the fall time slope, depolarization peak of the membrane remained constant.

$$y(mV) = -1.34 + 4.89 \ln \left(x \left(\frac{mW}{cm^2 ms} \right) \right)$$
 (6)

$$y(mV) = 0.36 + 1.00 \ln \left(x \left(\frac{mW}{cm^2 ms} \right) \right)$$
 (7)

4. Conclusion

In this study, we showed that modulation of rise and fall time slopes of light pulse waveforms control the direction and strength of currents generated by the photocapacitor. These capacitive currents facilitated high-level modulation of depolarization and hyperpolarization of the membrane potential. The control over hyperpolarization and depolarization by light can lead to an effective strategy for therapeutic purposes. Depending on the type of neural disorder, activation or silencing of neural activity is required. For example, Parkinson's disease requires depolarization of neural tissues to evoke action potential; on the other hand, in the case of epilepsy, suppression of neural activity is required. Moreover, since the maximum intensity levels illuminated at substrates are three orders of magnitude below maximum irradiance level for retinal cells, the control of capacitive currents via waveform shaping can be useful for retinal prosthetics as well. The proposed method was investigated on SHSY-5Y cell lines. In the future studies, the investigation of light pulse waveform control on the excitation and inhibition of neural activity on primary neural cell lines are the follow-up studies. If any photochemical or thermal damage would be observed on any tissue, the illumination powers and gradients can be optimized to obtain safe illumination conditions, which may influence the repetition frequency. Our results pave the way toward non-genetic and safe light-activated implants for superior optical control of neural activity.

Funding

(ERC) under the European Union Horizon 2020 Research and Innovation Programme (Grant agreement no. 639846).

Acknowledgments

The authors thank to Dr. Baris Yagci for the SEM measurement.

Disclosures

The authors declare no conflicts of interest.

References

- 1. J. Rivnay, H. Wang, L. Fenno, K. Deisseroth, and G. G. Malliaras, "Next-generation probes, particles, and proteins for neural interfacing," Sci. Adv. 3(6), e1601649 (2017).
- W. M. Grill and C. C. McIntyre, "Extracellular excitation of central neurons: implications for the mechanisms of deep brain stimulation," Thalamus Relat. Syst. 1(3), 269–277 (2001).doi:

- Q. Yang, D. Song, and H. Qing, "Neural changes in Alzheimer's disease from circuit to molecule: Perspective of optogenetics," Neurosci. Biobehav. Rev. 79, 110–118 (2017).
- T.-I. Kim, J. G. McCall, Y. H. Jung, X. Huang, E. R. Siuda, Y. Li, J. Song, Y. M. Song, H. A. Pao, and R.-H. J. S. Kim, "Injectable, cellular-scale optoelectronics with applications for wireless optogenetics," Science 340(6129), 211–216 (2013).
- 5. E. S. Boyden, "Optogenetics and the future of neuroscience," Nat. Neurosci. 18(9), 1200-1201 (2015).
- X. Han and E. S. Boyden, "Multiple-color optical activation, silencing, and desynchronization of neural activity, with single-spike temporal resolution," PLoS One 2(3), e299 (2007).
- J. S. Wiegert, M. Mahn, M. Prigge, Y. Printz, and O. Yizhar, "Silencing neurons: tools, applications, and experimental constraints," Neuron 95(3), 504–529 (2017).
- D. R. Merrill, M. Bikson, and J. G. Jefferys, "Electrical stimulation of excitable tissue: design of efficacious and safe protocols," J. Neurosci. Methods 141(2), 171–198 (2005).
- B. S. Wilson, C. C. Finley, D. T. Lawson, R. D. Wolford, D. K. Eddington, and W. M. Rabinowitz, "Better speech recognition with cochlear implants," Nature 352(6332), 236–238 (1991).
- 10. A. L. Benabid, "Deep brain stimulation for Parkinson's disease," Curr. Opin. Neurobiol. 13(6), 696–706 (2003).
- 11. T. R. Deer, N. Mekhail, D. Provenzano, J. Pope, E. Krames, M. Leong, R. M. Levy, D. Abejon, E. Buchser, and A. Burton, "The Appropriate Use of Neurostimulation of the Spinal Cord and Peripheral Nervous System for the Treatment of Chronic Pain and Ischemic Diseases: The N euromodulation A ppropriateness C onsensus C ommittee," Neuromodulation: Technology at the Neural Interface 17(6), 515–550 (2014).
- E. Zrenner, K. U. Bartz-Schmidt, H. Benav, D. Besch, A. Bruckmann, V.-P. Gabel, F. Gekeler, U. Greppmaier, A. Harscher, and S. Kibbel, "Subretinal electronic chips allow blind patients to read letters and combine them to words," Proc. R. Soc. London, Ser. B 278(1711), 1489–1497 (2011).
- D. E. Sanabria, L. A. Johnson, Y. Yu, Z. Busby, S. Nebeck, J. Zhang, N. Harel, M. D. Johnson, G. F. Molnar, and J. L. J. B. Vitek, "Suppressing and amplifying neural oscillations in real-time using phase-locked electrical stimulation: concept, optimization and in-vivo testing," bioRxiv (2020).
- D. B. McCreery, T. G. Yuen, W. F. Agnew, and L. A. J. I. T. O. B. E. Bullara, "A characterization of the effects on neuronal excitability due to prolonged microstimulation with chronically implanted microelectrodes," IEEE Trans. Biomed. Eng. 44(10), 931–939 (1997).
- M. Eickenscheidt, M. Jenkner, R. Thewes, P. Fromherz, and G. J. J. O. N. Zeck, "Electrical stimulation of retinal neurons in epiretinal and subretinal configuration using a multicapacitor array," J. Neurophysiol. 107(10), 2742–2755 (2012).
- H. Bahmani Jalali, M. Mohammadi Aria, U. M. Dikbas, S. Sadeghi, B. Ganesh Kumar, M. Sahin, I. H. Kavakli, C. W. Ow-Yang, and S. Nizamoglu, "Effective neural photostimulation using indium-Based type-II quantum dots," ACS Nano 12(8), 8104–8114 (2018).
- 17. D. Rand, M. Jakešová, G. Lubin, I. Vebraite, M. David-Pur, V. Đerek, T. Cramer, N. S. Sariciftci, Y. Hanein, and E. D. J. A. M. Głowacki, "Direct electrical neurostimulation with organic pigment photocapacitors," Adv. Mater. 30(25), 1707292 (2018).
- 18. M. Jakešová, M. S. Ejneby, V. Đerek, T. Schmidt, M. Gryszel, J. Brask, R. Schindl, D. T. Simon, M. Berggren, and F. Elinder, "Optoelectronic control of single cells using organic photocapacitors," Sci. Adv. 5(4), eaav5265 (2019).
- O. S. Abdullaeva, M. Schulz, F. Balzer, J. R. Parisi, A. Lützen, K. Dedek, and M. Schiek, "Photoelectrical stimulation of neuronal cells by an organic semiconductor-electrolyte interface," Langmuir 32(33), 8533–8542 (2016).
- Y. Jiang, X. Li, B. Liu, J. Yi, Y. Fang, F. Shi, X. Gao, E. Sudzilovsky, R. Parameswaran, and K. Koehler, "Rational design of silicon structures for optically controlled multiscale biointerfaces," Nat. Biomed. Eng. 2(7), 508–521 (2018).
- S. B. Srivastava, R. Melikov, M. M. Aria, U. M. Dikbas, I. H. Kavakli, and S. J. P. R. A. Nizamoglu, "Band Alignment Engineers Faradaic and Capacitive Photostimulation of Neurons Without Surface Modification," Phys. Rev. Appl. 11(4), 044012 (2019).
- 22. B. Boveja, "Method and system for modulating the vagus nerve (10th cranial nerve) using modulated electrical pulses with an inductively coupled stimulation system," (Google Patents, 2003).
- A. M. Marzouk, A. Stanitzki, and R. Kokozinski, "Towards pulse-density modulated functional electrical stimulation of neural cells with passive membranes," in *PRIME 2012; 8th Conference on Ph. D. Research in Microelectronics & Electronics (VDE2012)*, pp. 1–4.
- I. Schoen and P. J. B. J. Fromherz, "The mechanism of extracellular stimulation of nerve cells on an electrolyte-oxide-semiconductor capacitor," Biophys. J. 92(3), 1096–1111 (2007).
- N. K. Elumalai, A. J. E. Uddin, and E. Science, "Open circuit voltage of organic solar cells: an in-depth review," Energy Environ. Sci. 9(2), 391–410 (2016).